1-5-2007

CO_2-Forced Climate and Vegetation Instability During Late Paleozoic Deglaciation

Isabel P. Montañez
University of California, Davis, montanez@geology.ucdavis.edu

Neil J. Tabor
Southern Methodist University, Dallas, TX

Deb Niemeier
University of California, Davis

William A. DiMichele
Smithsonian Museum of Natural History, Washington, DC

Tracy D. Frank
University of Nebraska-Lincoln, tfrank2@unl.edu

See next page for additional authors

Published in *Science*, vol. 315. no. 5808 (January 5, 2007), pp. 87 - 91; doi: 10.1126/science.1134207 http://www.sciencemag.org/cgi/content/full/315/5808/87

Submitted August 22, 2006; accepted November 20, 2006.

CO_2-Forced Climate and Vegetation Instability During Late Paleozoic Deglaciation

Isabel P. Montañez,[1] Neil J. Tabor,[2] Deb Niemeier,[3] William A. DiMichele,[4] Tracy D. Frank,[5] Christopher R. Fielding,[5] John L. Isbell,[6] Lauren P. Birgenheier,[5] and Michael C. Rygel [5]

1 Department of Geology, University of California, Davis, CA 95616, USA
2 Department of Geological Sciences, Southern Methodist University, Dallas, TX 75275, USA
3 Department of Civil and Environmental Engineering, University of California, Davis, CA 95616, USA
4 Department of Paleobiology, Smithsonian Museum of Natural History, Washington, DC 20560, USA
5 Department of Geosciences, 214 Bessey Hall, University of Nebraska–Lincoln, Lincoln, NE 68588, USA
6 Department of Geosciences, University of Wisconsin, Post Office Box 413, Milwaukee, WI 53201, USA

Present address for M. C. Rygel: Department of Geology, State University of New York, College at Potsdam, Potsdam, NY 13676, USA

Corresponding author — I. P. Montañez, email montanez@geology.ucdavis.edu

Abstract

The late Paleozoic deglaciation is the vegetated Earth's only recorded icehouse-to-greenhouse transition, yet the climate dynamics remain enigmatic. By using the stable isotopic compositions of soil-formed minerals, fossil-plant matter, and shallow-water brachiopods, we estimated atmospheric partial pressure of carbon dioxide (pCO_2) and tropical marine surface temperatures during this climate transition. Comparison to southern Gondwanan glacial records documents covariance between inferred shifts in pCO_2, temperature, and ice volume consistent with greenhouse gas forcing of climate. Major restructuring of paleotropical flora in western Euramerica occurred in step with climate and pCO_2 shifts, illustrating the biotic impact associated with past CO_2-forced turnover to a permanent ice-free world.

A decade of studying Pleistocene ice cores has unequivocally documented a strong coupling of atmospheric partial pressure of CO_2 (pCO_2) and surface temperatures with changing global ice volume (1, 2). Although the precise mechanistic link between atmospheric greenhouse gases and climate is debated, there remains little doubt that high concentrations of atmospheric CO_2 have strongly amplified Earth's past climates. Anthropogenic CO_2 emissions have increased atmospheric CO_2 to concentrations higher than at any time in at least the past 650,000 years and could increase it to more than 2000 parts per million by volume (ppmv) as accessible fossil fuel reservoirs are exhausted (3). The last time such concentrations were seen on Earth was at the onset of our modern icehouse [~40 to 34 million years ago (Ma)], a transition from ice-free to glacial conditions characterized by repeated C cycle perturbation, large magnitude changes in atmospheric pCO_2, and major ephemeral warmings (4, 5). As our climate system departs from the well-studied Pleistocene glacial-interglacial cycles, a deep-time perspective of pCO_2-climate-glaciation linkages is essential for a fuller understanding of what may be the Earth's most epic deglaciation.

We present here the results of a multipronged investigation that provides evidence for significantly changing atmospheric CO_2 concentrations and surface temperatures during a 40-million-year period of the late Paleozoic (~305 to 265 Ma), which encompasses the deterioration of the most widespread and long-lived icehouse of the last half-billion years (6). This global warming event accompanied a permanent transition to an ice-free world, a condition that arguably lasted until the current glacial state. These results, when integrated with a newly emerging glaciation history for southern Gondwana (7–11), indicate strong linkages between pCO_2, climate, and ice-mass dynamics during the final stages of the Late Paleozoic Ice Age (end of LPIA).

Integration of these climate proxy records with our newly developed tropical paleobotanical records shows repeated climate-driven ecosystem restructuring in western paleo-equatorial Euramerica.

The CO_2 contents of ancient atmospheres can be estimated from the carbon stable isotope values ($\delta^{13}C$) of ancient soil-formed carbonates and goethites with an uncertainty of ≤ ±500 ppmv (12, 13). These minerals are the proxy of choice when pCO_2 is high (≥ 1000 ppmv), whereas the method's sensitivity decreases at lower pCO_2 (<800 ppmv) (14, 15). The precision of pCO_2 estimates reflects the variable assumptions used for each pCO_2 calculation (16), which can be further refined if the $\delta^{13}C$ of coexisting organic matter is available and if quantitative estimates of paleosoil-respired CO_2 content and paleotemperatures can be inferred from modern analogs or independently derived geochemical proxies (15).

To reconstruct atmospheric CO_2 during the end of the LPIA, we measured the $\delta^{13}C$ values of soil-formed calcites ($\delta^{13}C_{carb}$) collected from mature, well-drained profiles from the Eastern Shelf of the Midland Basin; the Pedregosa, Anadarko, and Paradox Basins; and the Grand Canyon Embayment of western paleoequatorial Euramerica (Figure S1 and table S1) (17). We consider measured paleosol $\delta^{13}C_{carb}$ values to be a robust proxy of soil-water CO_2 during formation, given the lack of evidence for mineral recrystallization and overgrowth and their overall shallow and low-temperature burial histories (18). Furthermore, we consider the $\delta^{13}C$ of well-preserved fossil plant matter ($\delta^{13}C_{org}$) tobea faithful proxy of the C isotope composition of soil-respired CO_2 and, in turn, of atmospheric CO_2 (19, 20). Compression and permineralized fossil plants, cuticles, coal, and charcoal were collected from mudstone deposits of abandoned fluvial channels and floodplains, which are stratigraphically intercalated (on a sub-10-m resolution) with carbonate-bearing paleosols (table S2). The use of measured $\delta^{13}C_{org}$ rather than penecontemporaneous marine carbonates as a proxy of atmospheric $\delta^{13}C$ reflects a growing appreciation of local-scale C cycling effects on the $\delta^{13}C$ values of epicontinental marine carbonates (21). The terrestrial $\delta^{13}C_{carb}$ and $\delta^{13}C_{org}$ time series have an average sampling interval of <1 million years (My) and define long-term trends that exhibit systematic variability (Figure 1, A and B). That the long-term $\delta^{13}C_{org}$ trend records first-order variations in atmospheric $\delta^{13}C$ is supported by its similarity to time-equivalent $\delta^{13}C_{org}$ records of Permo-Carboniferous coals from the North China Platform (22) and by a narrow range, throughout the study area, in the ratio of intracellular, *pi*, and atmospheric, *pa*, partial pressures of CO_2 in paleoflora [0.46 to 0.57 ± 0.3 (2 SE)], which were estimated by using measured $\delta^{13}C_{org}$ values of fossil plants and $\delta^{13}C_{carb}$ values of contemporaneous marine brachiopods (17). These factors indicate that changes in

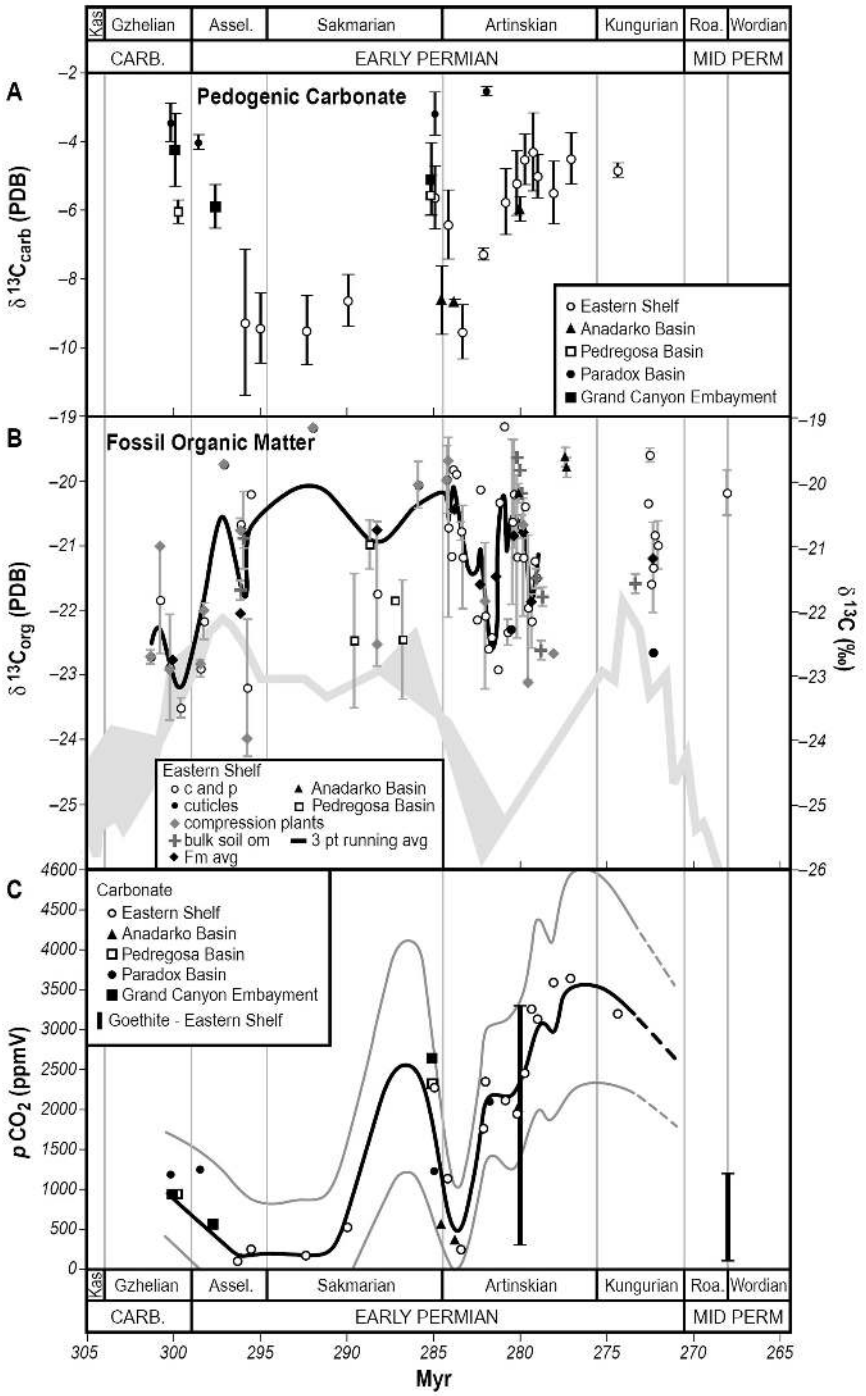

Figure 1. Temporal distribution of carbonate (**A**) and fossil plant (**B**) $\delta^{13}C$ values used to construct best estimate of Permo-Carboniferous atmospheric pCO_2 (**C**). Individual points in (A) and (B) are the average of analyses from suites of contemporaneous paleosols (from 5 to 18) and associated plant localities (from 3 to 21); "cand p" encompasses all compression and permineralized plant matter, coals, and charcoals. Vertical bars are ±2 SE around the mean. PDB, Pee Dee belemnite. (B) Solid curve is three-point weighted running average through samples from the Eastern Shelf, Midland Basin. Gray band is $\delta^{13}C_{org}$ of Permo-Carboniferous coals from three correlated successions in North China Platform (22). Overlapping $\delta^{13}C_{org}$ trends but different $\delta^{13}C_{org}$ values are interpreted to reflect overall wetter conditions for the North China Platform relative to western paleoequatorial Euramerica in the Permian. Data and pCO_2 presented on an age model (51) developed for the terrestrial composite section by linearly interpolating between known biostratigraphic boundaries. (C) Best estimate of paleo-pCO_2 (black curve) from Monte Carlo simulation of chronostratigraphically well-constrained sample populations; uncertainty in pCO_2 estimates (gray curves) reflects variability in $\delta^{13}C_{carb}$ and $\delta^{13}C_{org}$, interpreted to record inter- and intrabasinal variations in soil conditions, vegetation, and climate. Vertical bars are published goethite-based CO_2 estimates from the same set of paleosols (25).

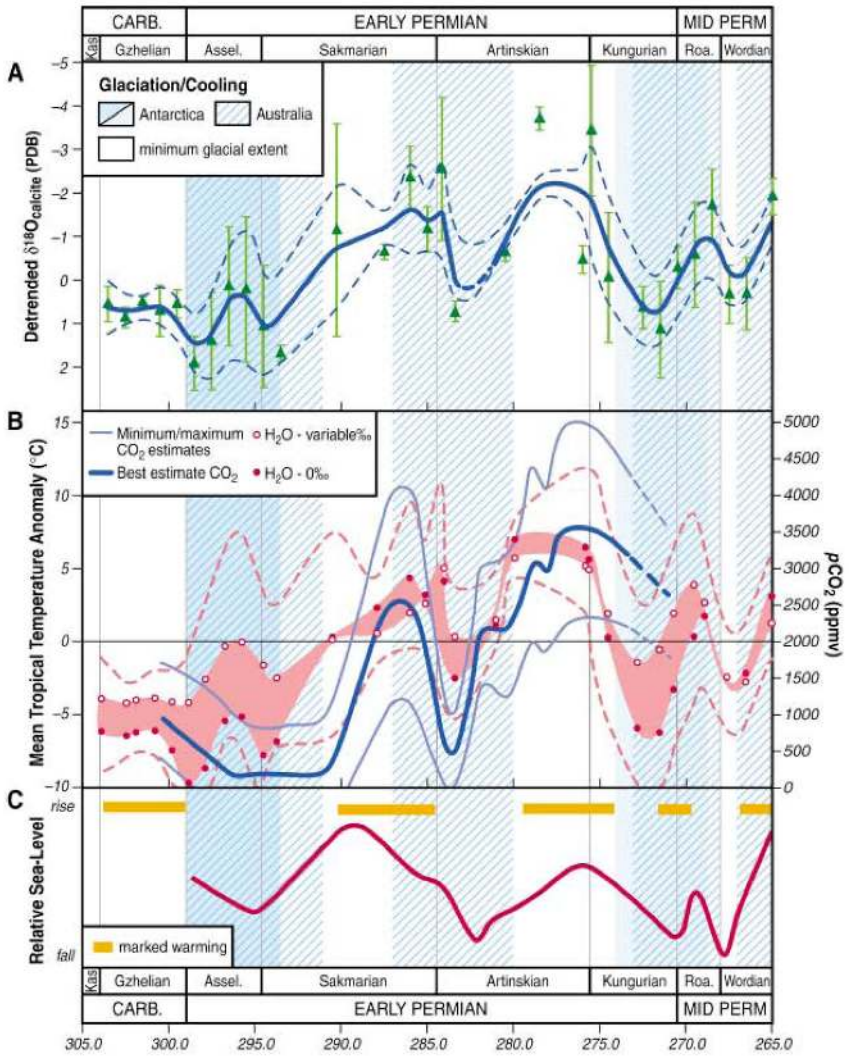

Figure 2. Relationship among Permo-Carboniferous pCO_2, climate, and cryosphere. Temporal distribution of glacial maxima and/or cool periods based on stratigraphic distribution of diamictites, rhythmites, and dropstone and keel turbate structures in Antarctica and Australian glacigenic deposits (10, 11). (**A**) Three-point weighted running average (blue curve) and ±2 SE (dashed curves) of detrended $\delta^{18}O_{brachiopod}$ values binned into 1- to 3-My windows (green triangles). Error bars indicate ±2 SE around the mean $\delta^{18}O_{brachiopod}$ values. (**B**) Inferred paleotropical SSTs (red interval) (40) are reported as temperature anomalies given the potential effects of local and regional environmental and diagenetic influences on brachiopod $\delta^{18}O$. Paleo-SST anomalies (relative to 17.5° C) were calculated from a three-point weighted running average (± 2 SE) through $\delta^{18}O$-based paleotemperature estimates (table S5). Blue curves are best estimate (heavy) and uncertainty (light) of paleo-pCO_2.(**C**) Relative sea-level curve compiled from (8, 53); distribution of warm intervals, from (7–9) and (34).

in the study area were secondary to atmospheric $\delta^{13}C$ in influencing measured fossil-plant $\delta^{13}C_{org}$ values.

Ranges of paleosoil-respired CO_2 content were inferred from the morphologies of suites of contemporaneous paleosols (23) by comparison with modern analogs, addressing a major source of uncertainty in previous applications of the CO_2 paleobarometer (table S3) (14, 15). Paleosol temperatures were inferred from the oxygen and hydrogen isotopic compositions of pedogenic phyllosilicates and Fe oxides obtained from the same set of paleosols (18, 24). The best estimate of paleoatmospheric pCO_2 was defined by using Monte Carlo simulation involving 1000 randomly drawn samples for each variable for each time-location combination (17). Monte Carlo simulation uses random sampling techniques to stochastically solve physical process problems, in this case quantitatively estimating paleo-pCO_2 and the associated uncertainty by integrating across all of the inferred and measured input variables.

Modeled CO_2 concentrations (Figure 1C and table S4) define a long-term rise from an average of present atmospheric levels (PAL = 280 ppmv) in the earliest Permian to values of up to 3500 ppmv by the late Early Permian. A substantial decline in pCO_2 into the early Middle Permian is corroborated by independently derived goethite-based estimates of Permian pCO_2 (25). A short-lived (~2 My) drop in pCO_2 to near PAL, defined by contemporaneous paleosols, punctuates the Early Permian rise. Modeled pCO_2 suggests that PAL values were limited to the earliest Permian after latest Carboniferous levels of up to 1000 ppmv, in accord with pCO_2 inferred from marine carbonate $\delta^{13}C$ (26) and with southern Gondwanan sedimentologic and geochemical evidence for latest Carboniferous warming (9, 27). Our record refines the structure of well-established pCO_2 reconstructions, which indicate sustained PAL values throughout much of the Permo-Carboniferous (15, 28, 29). The higher-frequency oscillations revealed by this study would be below the temporal resolution (5 to 20 My time-averaging) of those long-term CO_2 records.

In order to evaluate the nature of the CO_2-climate relationship, we developed a time-equivalent record of paleotropical sea-surface temperatures (SSTs) by using $\delta^{18}O$ values from a global compilation of well-preserved latest Carboniferous through Middle Permian tropical shallow-water brachiopods (table S5) (30); brachiopods have diagenetically resistant, low-Mg calcitic shells that incorporate oxygen isotopes in equilibrium with seawater (31). The residual brachiopod $\delta^{18}O$ record (Figure 2A) displays clear isotopic fluctuations, with intervals of maximum values corresponding to Permian glacial maxima or marked coolings in Antarctica and/or Australia (10, 11) and, to the degree afforded by geochronologic dates, with the younger periods of inferred glacial maxima in the Karoo Basin (8, 32), southern Argentina (9), and Tasmania (33). Intervals of minimum $\delta^{18}O_{carb}$ values correspond with independently inferred periods of marked warming and sea-level rise (7–9, 34)(Figure 2C).

Inferring secular paleotemperatures from $\delta^{18}O_{carb}$ requires careful consideration of the compound effects on values of continental ice volume, local hydrography, and SST, as well as any vital effects and postdepositional alteration (31, 35). The eustatic component in the Permo-Carboniferous brachiopod $\delta^{18}O$ record due to ice volume variability likely accounts for far less than 2 per mil (‰) of the observed $\delta^{18}O$ variation given reconstructed amplitudes (10 to <100 m) of Permo-Carboniferous glacioeustasy (10) and an O isotope composition of seawater ($\delta^{18}O_{sw}$)–sea level relationship of 0.1‰ per 10 m of sea level change (36). The residual secular $\delta^{18}O_{carb}$ signal is interpreted to record changes in temperature, salinity, and pH. Local hydrographic variations in tropical epicontinental seas would have dampened the magnitude of $\delta^{18}O_{carb}$ shifts, given hypothe-sized heightened freshwater discharge to continental shelves (decreased salinity and lowered $\delta^{18}O_{sw}$) during late Paleozoic periods of maximum glaciation, and increased evaporation (increased salinity and $\delta^{18}O_{sw}$) during drier, highly seasonal

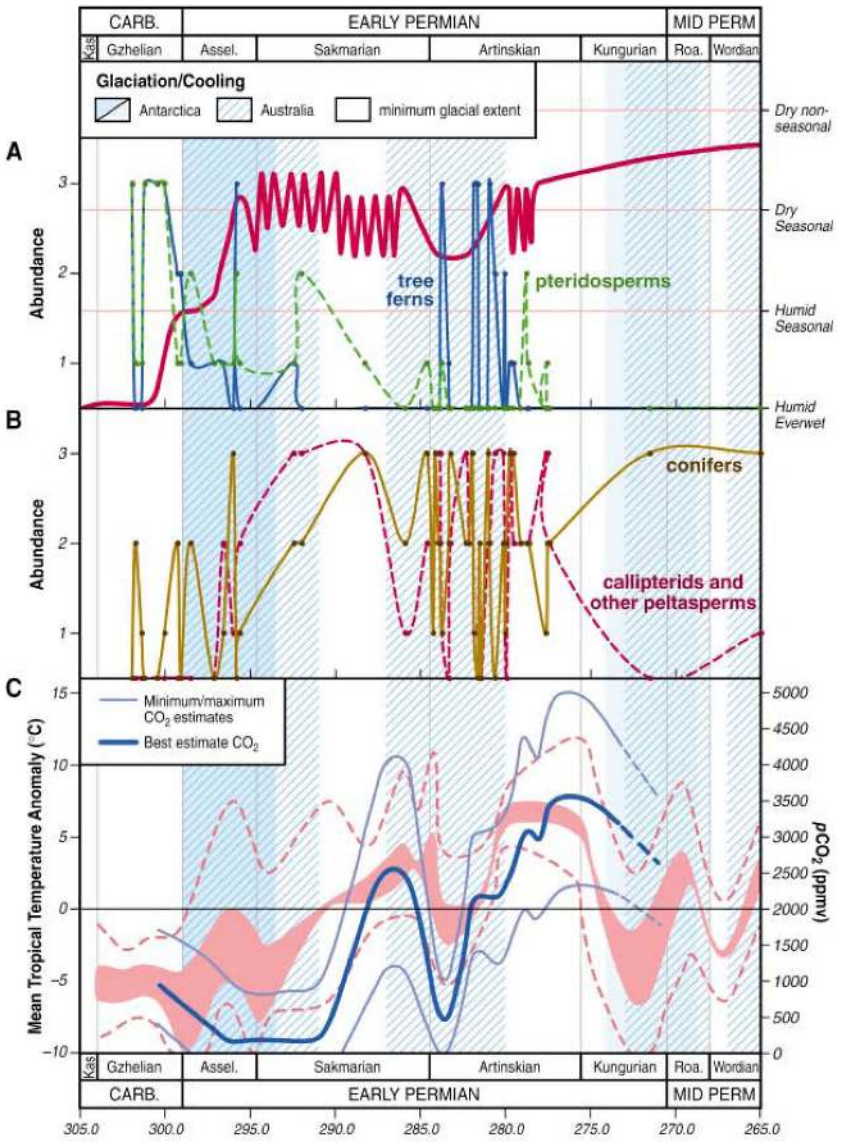

Figure 3. Patterns of abundance change in major flora of study area (**A** and **B**) and comparison to independently derived Permo-Carboniferous climate and pCO_2 (**C**). Plants from 49 sampling localities on the Eastern Shelf, Midland Basin, are rank ordered: 1, rare (occurs in <10% of sampling quadrats at any given locality), 2, common (occurs in 10 to 50% of sampling quadrats), and 3, abundant (occurs in >50% of sampling quadrats). (**A**) Tree ferns and pteridosperms are hygromorphic and occur in deposits with sedimentologic and pedogenic indicators of everwet to subhumid seasonal conditions. Red climate curve for paleoequatorial western Euramerica defined by using soil moisture regimes and degree of seasonality inferred from paleosol morphologies (23); zigzag pattern indicates short-term (10^3 to 10^5 year) climate cycles inferred from intervals of polygenetic soils that exhibit climatically out-of-phase superposition of calcic and argillic horizons. (**B**) Conifers and peltasperms are xeromorphic and typically are found in association with sedimentologic and pedogenic indicators of moisture limitation.

glacial minima (36). Moreover, paleo-SSTs under elevated pCO_2 may be under-estimated by up to 2°C, given that lowered seawater pH would have shifted $\delta^{18}O_{carb}$ to less negative values (38, 39).

The amplitudes of the reconstructed SSTshifts (40) indicate substantial changes in the mean state of tropical climate during the end of the LPIA, with glacial tropical oceans at least 4° to 7°C cooler than those of intervening glacial minima (Figure 2B). Inferred periods of elevated tropical SSTs and pCO_2 coincide with independently recognized intervals of warmer temperate conditions in high-latitude southern Gondwana (Figure 2C) indicated by the accumulation of nonglacial sediments, including extensive kaolin and bauxite deposits in Australia during peak (Artinskian) warming and pCO_2 (7) and increased faunal diversity in Australia and South America (7, 11, 41). The covariance among inferred shifts in paleotropical SSTs, pCO_2, and variations in high-latitude Gondwanan glaciation and climate implies a strong CO_2-climate-glaciation linkage during the Permian. Although our coupled records suggest atmospheric CO_2 may have played a direct role in forcing Early to Middle Permian climate and ice mass stability, a determination of phase relationships between these parameters is precluded by the uncertainties in the age models. The inferred variations in tropical SSTs between periods of glacial maxima and minima, however, are consistent with the range predicted by Permian climate simulations for a change in radiative CO_2 forcing from 1 to 8 PAL (42).

Permo-Carboniferous plant assemblages from western paleoequatorial Euramerica archive a mechanistic vegetational response to late Paleozoic pCO_2 and climate change. Reconstructed plant communities from the same terrestrial successions that host the pedogenic mineral-bearing paleosols document major dominance-diversity changes corresponding one-for-one to inferred changes in paleotropical climate, pCO_2, and glacial extent (Figure 3 and table S6). Four tropical biomes appear in succession, composed of increasingly xeromorphic species, representing progressively more seasonally moisture-stressed environments. These biomes are floristically distinct, sharing only a few opportunistic ferns and sphenopsids (43). Typical latest Carboniferous flora, rich in marattialean ferns, medullosan pteridosperms, sphenopsids, and sigillarian lycopsids, was replaced essentially instantaneously by one rich in conifers {*Walchia* and *Ernestiodendron*; compare with *Brachyphyllum* (44), callipterids (*Rhachiphyllum*), cycadophytes (*Russellites*), and other seed plants [*Cordaites, Sphenopteridium* (45)]}. This floristic shift is synchronous with an abrupt continental climate transition from everwet to semi-arid conditions (Figure 3A), characterized by increased temperatures (18, 24) and seasonal moisture availability inferred from paleosol morphologies (23).

Conifers and callipterids diversified in seasonally dry habitats during the initial Early Permian (Sakmarian) rise in CO_2 and the warm period of glacial minima, spatially replacing the tree fern–rich and the pteridosperm-rich wetland floras (Figure 3). Tree fern–rich floras reappeared during wetter, cooler conditions of the mid-Early Permian (Artinskian) glaciation, stratigraphically intercalated but not mixed, with conifer-callipterid floras. These two glacial floras show limited species overlap and oscillated at the 10^3- to 10^5-year scale, reflecting short-lived pluvials (46). Dramatic floristic changes also occurred during the cold period at the close of the Early Permian (Kungurian), with the migration into lowland basins of unique seed-plant assemblages not observed again until the Late Permian (conifers) and the Mesozoic (cycads) (47). These temporally successive floras tracked climatic conditions and contained progressively more evolutionarily

advanced lineages. This suggests that evolutionary innovation, the appearance of new plant body plans, occurred in extrabasinal areas and was revealed by climate-driven floral migration into lowland basins.

The history of latest Carboniferous to Middle Permian climate provides a unique deep-time perspective on the precarious balance between icehouse and greenhouse states during major climate transitions, which are coupled to changing atmospheric CO_2 content. Maximum expansion of Gondwanan continental ice sheets occurred during earliest Permian time (10) under the lowest paleoatmospheric CO_2 levels and paleotropical SSTs. Widespread Early Permian (mid-Sakmarian) collapse of ice sheets (8, 10) coincided with the onset of rising atmospheric CO_2 levels, after which time tropical SSTs and pCO_2 rose. Subsequent glacial influence was restricted to eastern Australia (6), with resurgent ice masses occurring during three more episodes (11) of lowered atmospheric pCO_2 before the permanent transition to an ice-free world (260 Ma). Our study indicates that ice buildup in Australia during subsequent cold periods, however, was progressively less widespread, with the two youngest glacials generally confined to local valleys or mountain ice caps along the polar margin of Australian Gondwana. Notably, SSTs and pCO_2 did not return to earliest Permian levels during these post-Sakmarian glacial periods.

Our reconstructed pCO_2, paleotemperatures, and inferred glacial history depict an Early Permian atmosphere that systematically increased from PAL to levels similar to those predicted to exist if fossil fuels are exhausted. Although global-scale deglaciation was unrelenting under rising Early Permian atmospheric CO_2, transient periods of icehouse stability and glacial resurgence returned during short-lived intervals of low pCO_2, perhaps until a CO_2 threshold and greenhouse stability precluded the reestablishment of glacial conditions [compare with (48)]. This late Paleozoic climate behavior mimics, in reverse, the magnitude and temporal scale of atmospheric CO_2 changes and ephemeral warmings that foreshadowed the transition into our present glacial state (4, 5), further documenting the degree of climate variability, carbon cycle perturbation, and tropical ecosystem restructuring that has been associated with past CO_2-forced climate transitions.

References and Notes

1. J. R. Petit *et al.*, *Nature* **399**, 429 (1999).
2. U. Siegenthaler *et al.*, *Science* **310**, 1313 (2005).
3. L. R. Kump, *Nature* **419**, 188 (2002).
4. M. Pagani, J. C. Zachos, K. H. Freeman, B. Tipple, S. Bohaty, *Science* **309**, 600 (2005); published online 16 June 2005 (10.1126/science.1110063).
5. A. Tripati, J. Backman, H. Elderfield, P. Ferretti, *Nature* **436**, 341 (2005).
6. L. A. Frakes, J. E. Francis, J. I. Syktus, *Climate Modes of the Phanerozoic* (Cambridge Univ. Press, Cambridge, 1992).
7. J. M. Dickins, *Palaeogeogr. Palaeoclimatol. Palaeoecol.* **125**, 185 (1996).
8. H. Stollhofen, I. G. Stanistreet, B. Bangert, H. Grill, *Palaeogeogr. Palaeoclimatol. Palaeoecol.* **161**, 127 (2000).
9. C. R. Gonzalez, *Palaeogeogr. Palaeoclimatol. Palaeoecol.* **79**, 275 (1990).
10. J. L. Isbell, M. F. Miller, K. L. Wolfe, P. A. Lenaker, *Geol. Soc. Am. Spec. Pap. 370* (2003), pp. 5–24.
11. A. T. Jones, C. R. Fielding, *Geology* **32**, 153 (2004).
12. T. E. Cerling, in *Palaeoweathering, Palaeosurfaces, and Related Continental Deposits*, M. Thiry, R. Simon-Coinçon, Eds. (Blackwell, Cambridge, 1999), pp. 43–60.
13. C. J. Yapp, H. Poths, *Nature* **355**, 342 (1992).
14. D. L. Royer, R. A. Berner, D. J. Beerling, *Earth Sci. Rev.* **54**, 349 (2001).
15. D. D. Ekart, T. E. Cerling, I. P. Montañez, N. J. Tabor, D. J. Beerling, *Am. J. Sci.* **299**, 805 (1999).
16. CO_2 paleobarometer input parameters include, from most to least sensitive: (i) soil-respired CO_2 content (S_z in ppmv), typically assumed to be constant, (ii) the C isotopic composition of soil-respired ($\delta^{13}C_{\varnothing}$) and atmospheric ($\delta^{13}C_A$) CO_2, both typically derived from broadly contemporaneous marine carbonates, and (iii) temperature, typically held constant (~25°C). Pedogenic carbonate $\delta^{13}C$ is utilized as the proxy of $\delta^{13}C$ of total soil-CO_2. For goethite-based pCO_2 estimates, the measured concentration and $\delta^{13}C$ of the Fe(CO_3) OH component in pedogenic goethite are taken as proxies of ambient pCO_2 and $\delta^{13}C$, respectively, present during crystallization; $\delta^{13}C_{\varnothing}$ and $\delta^{13}C_A$ are inferred from marine carbonate proxies or fossil organic matter.
17. Materials and methods are available as supporting material on *Science* Online.
18. N. J. Tabor, I. P. Montañez, *Palaeogeogr. Palaeoclimatol. Palaeoecol.* **223**, 127 (2005).
19. The $\delta^{13}C_{org}$ values of matrix in calcic-paleosols and contemporaneous fossil-plant matter overlap (Figure 1B), indicating that the latter are representative of soil-respired CO_2 in carbonate-bearing paleosols. A $\delta^{13}C_{atm}$ proxy record was calculated assuming isotopic equilibrium fractionation ($\Delta_{atm\text{-}om}$ of 18.5‰) between paleoflora ($\delta^{13}C_{org}$) and atmospheric CO_2. Paleo-pCO_2 estimated using a 2‰ variation in $\Delta_{atm\text{-}om}$ falls within the uncertainty band shown on Figure 1C, reflecting the low sensitivity of the model to $\delta^{13}C_A$.
20. N. C. Arens, A. H. Jahren, R. Amundson, *Paleobiology* **26**, 137 (2000).
21. K. M. Panchuk, C. Holmden, S. A. Leslie, *J. Sediment. Res.* **76**, 200 (2006).
22. H. Zhang, G. Shen, Z. He, *Acta Geol. Sin.* **73**, 111 (1999).
23. N. J. Tabor, I. P. Montañez, *Sedimentology* **51**, 851 (2004).
24. N. J. Tabor, *Earth Planet. Sci. Lett.*, in press.
25. N. J. Tabor, C. J. Yapp, I. P. Montañez, *Geochim. Cosmochim. Acta* **68**, 1503 (2004).
26. M. R. Saltzman, *Geology* **31**, 151 (2003).
27. K. Scheffler, S. Hoernes, L. Schwark, *Geology* **31**, 605 (2003).
28. R. A. Berner, Z. Kothavala, *Am. J. Sci.* **301**, 182 (2001).
29. C. I. Mora, S. G. Driese, L. A. Colarusso, *Science* **271**, 1105 (1996).
30. Published $\delta^{18}O$ data are from biostratigraphically constrained and diagenetically screened calcitic brachiopods (31, 35, 49); $\delta^{18}O$ values < –8‰ were excluded. The $\delta^{18}O$ values were detrended to remove the effects of the long-term linear Phanerozoic trend by removing, from each data point, the least squares linear fit calculated using SPlus.
31. H. Mii, E. Grossman, T. E. Yancey, *Geol. Soc. Am. Bull.* **111**, 960 (1999).
32. B. Bangert, R. Armstrong, H. Stollhofen, V. Lorenz, *J. Afr. Earth Sci.* **29**, 33 (1999).
33. M. R. Banks, in *Earth's Pre-Pleistocene Glacial Records*, M. J. Hambrey, W. B. Harland, Eds. (Cambridge Univ. Press, Cambridge, 1981), pp. 495–501.
34. J. N. J. Visser, *Sedimentology* **44**, 507 (1997).
35. C. Korte, T. Jasper, H. W. Kozur, J. Veizer, *Palaeogeogr. Palaeoclimatol. Palaeoecol.* **224**, 333 (2005).
36. D. P. Schrag *et al.*, *Quat. Sci. Rev.* **21**, 331 (2002).
37. C. B. Cecil *et al.*, in *Climate Controls on Stratigraphy*, C. B. Cecil, T. N. Edgar, Eds. (SEPM Special Publication 77, Society for Sedimentary Geology, Tulsa, OK, 2003), pp. 151–180.
38. D. L. Royer, R. A. Berner, I. P. Montañez, N. J. Tabor, D. J. Beerling, *Geol. Soc. Am. Today* **14**, 3 (2004).
39. W. C. Beck, E. L. Grossman, J. W. Morse, *Geochim. Cosmochim. Acta* **69**, 3493 (2005).
40. Detrended $\delta^{18}O$ values were binned into 1- to 3-My windows. Average values (±2 SE) were translated to a range of paleotropical SSTs by using a quadratic equation (50) and a constant (0‰) or variable (–0.5 to + 1.5‰) $\delta^{18}O_{sw}$. The influence of local and environmental factors and diagenesis on the long-term $\delta^{18}O_{carb}$ trend is considered secondary, given the overlap in individual published datasets and Tethyan and Panthalassan brachiopod $\delta^{18}O$ values; secondary influences are likely recorded in the $\delta^{18}O_{brachiopod}$ variability within contemporaneous populations.
41. O. R. Lopez-Gamundi, in *Late Glacial and Postglacial Environmental Changes: Quaternary, Carboniferous-Permian, and Proterozoic*, I. P. Martini, Ed. (Oxford Univ. Press, Oxford, 1997), pp. 147–168.
42. A. M. E. Winguth *et al.*, *Paleoceanography* **17**, 1057 (2002).
43. W. A. DiMichele, R. B. Aronson, *Evolution* **46**, 807 (1992).
44. Compare with *Brachyphyllum* after S. H. Mamay, *U.S. Geol. Surv. Prof. Pap. 575-C* (1967), p. 120.
45. *Sphenopteridium*, after S. H. Mamay, *Am. J. Bot.* **79**, 1092 (1992).
46. W. A. DiMichele, N. J. Tabor, D. S. Chaney, W. J. Nelson, *Geol. Soc. Am. Spec. Pub. 299* (2006), pp. 223–248.
47. W. A. DiMichele, D. S. Chaney, W. H. Dixon, W. J. Nelson, R. W. Hook, *Palaios* **15**, 524 (2000).
48. L. R. Kump, *Nature* **436**, 333 (2005).
49. J. Veizer *et al.*, *Chem. Geol.* **161**, 59 (1999).
50. S. T. Kim, J. R. O'Neil, *Geochim. Cosmochim. Acta* **61**, 3461 (1997).
51. A chronostratigraphic framework for the Eastern Shelf of Texas (23) was used as the basis for the composite section into which other records were integrated with use of available biostratigraphy and lithostratigraphic correlation. Calibration of the Eastern Shelf succession to the Gradstein *et al.* 2004 geologic time scale (52) is based, for the study area, on the stratigraphic position of the stage boundaries determined by conodont, fusulinid, and ammonite biostratigraphy.
52. F. M. Gradstein, J. G. Ogg, A. G. Smith, Eds., *A Geologic Time Scale 2004* (Cambridge Univ. Press, Cambridge, 2005).
53. C. A. Ross, J. R. P. Ross, in *Sea-Level Changes: An Integrated Approach*, C. K. Wilgus *et al.*, Eds. (SEPM Special Publication 42, Society for Sedimentary Geology, Tulsa, OK, 1988), pp. 227–247.

PP-0126086, and ANT-0440919.

Supporting Material follows: **Materials and Methods**, **Figure S1**, and **Tables S1** to **S6**;
it can also be found online @ www.sciencemag.org/cgi/content/full/315/5808/87/DC1

SUPPLEMENTAL ONLINE MATERIAL for Montañez et al.

Materials & Methods

Calcite nodules and rhizoliths, phyllosilicates, and Fe-oxide samples were collected from at least 0.5 m beneath the surfaces of mature paleosols within latest Pennsylvanian through Middle Permian terrestrial successions shown in Figure S1. We present here only the methodology for analyses and CO_2 estimates not previously published. The methodology for C isotope analysis of goethites and their application to paleo-pCO_2 reconstruction are presented in detail in *S1*. The methodology for D and O isotope analysis of phyllosilicates and Fe-oxides and their application to continental paleo-temperature reconstruction are presented in *S2 – S4*.

Carbonate Stable Isotope Analysis: Micritic calcite exhibiting pedogenic micromorphologies (*S5*) and no evidence of secondary dissolution and reprecipitation based on petrographic criteria (*S6*) were microsampled using a Merchantek automated microsampler. Approximately 50 μg of carbonate were roasted at 375°C in vacuum for three hours to remove organics. Samples were analysed on a Fisons Optima IRMS using an Isocarb common acid bath autocarbonate system at 90°C at the Stan Margolis Stable Isotope Laboratory, University of California, Davis (UCD). External precision for the $\delta^{13}C$ measurements based on standards and replicates is better than ±0.06‰. Results are shown in Table S1.

Organic Matter Stable Isotope Analysis: Organic matter samples were hand-picked with cleaned metal probe and tweezers, cleaned in Nanopupre H_2O, and placed into acid-washed Pyrex test tubes. Samples were treated with 1 N HCl overnight at room temperature and then rinsed four times with Nanopupre H_2O to remove any carbonate and hydrolysable C. Between 60 and 100 μg of cleaned and dried sample was loaded in tin boats. C isotope analysis was carried out on an Isoprime isotope ratio mass spectrometer interfaced to a Carlo Erba elemental analyzer at the Plant Sciences Stable Isotope Laboratory and Dept. of Geology at UCD. External precision for the $\delta^{13}C$ measurements based on standards and replicates is better than ±0.3‰. Results are shown in Table S2.

Estimating Pi/Pa indices from Fossil Plant Matter: *Pi/pa*, the ratio of partial pressures of CO_2 in the substomatal cavity of plants and the atmosphere, is an established proxy of water-use efficiency of plant growth that is influenced by several environmental variables (*S7*). We estimated *pi/pa* ratios using the well-validated theoretical model of Farquhar *et al.* (*S8*) according to:

$$\text{Plant } \Delta^{13}C = a + (b - a) \text{ X } pi/pa,$$

where *a*, the fractionation that occurs during stomatal diffusion, is 4.4‰, and *b*, the kinetic fractionation that occurs during the fixation of CO_2 by Rubisco, is 27‰.

Plant $\Delta^{13}C$ was calculated using:

$$\Delta^{13}C = \frac{(\delta^{13}C_{atm} - \delta^{13}C_{plant\ matter})}{(1 + \delta^{13}C_{plant\ matter}/1000)}$$

Estimated *pi*/*pa* ratios throughout the 40-million year interval define a narrow range within each depositional basin (0.46 to 0.57 ±0.3 (2 std error of the mean) for the Eastern Shelf; 0.55 to 0.58 ±0.2 for the Pedregosa Basin; 0.48 to 0.56 ±0.02 for the Anadarko Basin), regardless of landscape or stratigraphic position. The low values record the overall dry conditions in the region and post-depositional alteration; their narrow range, however, is interpreted to record the low degree of geomorphic or environmental influence on fossil plant $\delta^{13}C_{org}$ values.

Monte Carlo Modeling: To estimate the best-fit and standard deviation curves for paleo-pCO_2 we used Monte Carlo simulation methods, which can be applied to evaluate statistical estimators with computational algorithms to simulate a population. For each of the individual time-location combinations (Table S3), data summary statistics were calculated for each variable used in the Monte Carlo simulation (details of modeling and error analysis presented in *S9*). In addition, variables were also assigned a statistical distribution. For each time-location combination, 1000 samples were drawn for each of the Monte Carlo variables to generate alternative scenarios. That is, each variable was assumed to be independent and values were randomly drawn based on assumed normal or uniform distributions. Together, these scenarios gave a range of possible solutions, some of which were considered more probable and some less probable. That is, the result is considered a distribution of results from which summary statistics (e.g., expected values) can be estimated. Once the sample of 1000 values had been generated for each time-location combination, individual pCO_2 values were calculated along with the overall mean and standard deviations (Table S4).

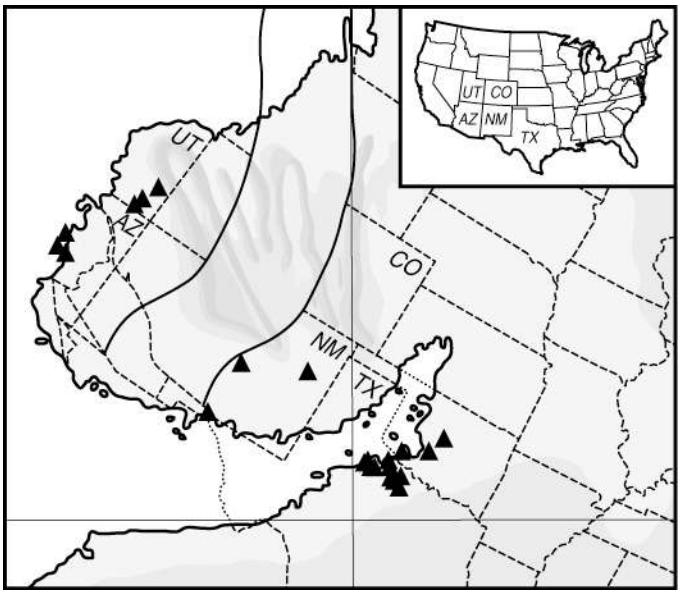

Figure S1. Location of sampled successions (triangles) on the Eastern Shelf of the Midland Basin (north-central TX) and the Pedregosa (south-central NM), southern Anadarko (south-central OK), Paradox (south-eastern UT), and Grand Canyon Embayment (north-western AZ). The "gap" intersecting NM and CO corresponds to inferred distance of shortening from Laramide and Sevier orogenies. The solid black lines

delineate the approximate position of the Early Permian coastlines along western paleoequatorial Pangaea (modified from *S10*).

Table S1. Pedogenic carbonate $\delta^{13}C$ values used for paleo-pCO_2 reconstruction.

Samples	**Age[1] (Ma)**	**$\delta^{13}C_{ped\ carb}$ measured**	**$\delta^{13}C_{ped\ carb}$ Avg. (±2 s.e.)**
Honaker Trail Fm, UT	300.3		-3.4 (±0.6)
HT 1A-1		-2.8	
HT 1B-1		-3.9	
HT3-1		-4.0	
HT 3A		-3.2	
HT2		-4.3	
HT1-1		-2.4	
HT1-2		-3.7	
HT1-3		-3.1	
Hermit Shale Fm, Kohl's Ranch, AZ	300.0		-4.2 (±1.1)
N1-1		-4.8	
N1-2		-3.7	
Bursum Fm, Socorro, NM	299.8		-6.1 (±0.3)
BF1-1		-5.7	
BF1-2		-6.7	
BF4-1		-5.9	
BF4-2		-5.8	
BF7		-6.1	
upper Halgaito Fm, AZ	298.6		-4.0 (±0.2)
HAL 1A		-4.0	
HAL 2		-4.1	
HAL 4A		-4.2	
HAL 7		-3.6	
HAL 9A		-3.4	
HAL 9B		-3.5	
HAL 12		-4.4	
HAL 15		-3.0	
HAL 17		-4.5	
HAL 18		-4.2	
HAL 22		-4.1	
HAL 25B		-4.1	
HAL 25B-B2		-4.2	
HAL 26		-3.9	
HAL 48		-4.7	
HAL 48 R		-4.5	

Table S1. continued

Samples	Age[1] (Ma)	$\delta^{13}C_{ped\ carb}$ measured	$\delta^{13}C_{ped\ carb}$ Avg. (±2 s.e.)
Hermit Shale Fm, south of Flagstaff, AZ	297.7		-5.9 (±0.6)
S2-1		-6.6	
S2-2		-6.7	
S4-1		-5.6	
S4-2		-5.2	
S4-3		-5.3	
middle Archer City Fm, stratotype (SS5), nc-TX	296.0		-9.3 (±2.1)
AC 27		-10.1	
AC 28		-10.9	
AC 29		-11.1	
AC 31		-5.3	
AC 32		-9.0	
upper Archer City Fm bonebed (SS8), nc-TX	295.1		-9.4 (±1.0)
ABBA 79 - 9C		-10.7	
ACBBH/R		-9.9	
ABBA 3C-1		-8.5	
ABBA 3C-2		-8.7	
basal Nocona Fm, coprolite bonebed, nc-TX	292.4		-9.5 (±1.0)
NBCX		-9.6	
NBC4-1		-8.2	
NBC4F		-10.6	
middle Nocona Fm, nc-TX	290.0		-8.6 (±0.8)
NLAD 99-1A		-8.3	
NLAD 99-1B		-8.3	
NLAD 2C		-9.4	
Abo Fm, Socorro to Las Cruces, NM	285.2		-5.6 (±0.6)
A7-1		-6.7	
A9-1		-6.2	
A10		-4.1	
A3-1		-4.5	
A3-2		-4.0	
A4-1		-6.3	
A4-2		-6.3	
A7-2		-6.0	
A8		-5.0	
A9-2		-6.1	
A9-3		-5.9	
upper Hermit Shale Fm, Nash Pt & Fossil Springs, AZ	285.1		-5.1 (±1.1)
NP2-1		-4.4	
NP2-2		-4.4	
HS1		-6.2	
HS5		-5.3	

Table S1. continued

Samples	Age[1] (Ma)	$\delta^{13}C_{ped\ carb}$ measured	$\delta^{13}C_{ped\ carb}$ Avg. (±2 s.e.)
Cedar Mesa Fm, se-UT	285.0		-3.2 (±0.6)
CM 1A		-2.1	
CM 2A		-4.4	
CM 5		-2.1	
CM3A-1		-4.0	
CM3B		-4.0	
CM3A-2		-3.0	
CM3B-2		-3.4	
CM5		-2.6	
uppermost Nocona Fm, lower Parkeys Oil Patch, nc- TX	285.0		-5.6 (±0.9)
NoPlat1		-5.9	
NoPlat 2C-H		-9.0	
NoPlat 2C-C		-5.9	
NoPlat 4J		-4.1	
NoPlat 4L		-5.2	
NoPlat 4P		-5.2	
NoPlat 4O-1		-5.1	
NoPlat 4O-2		-5.2	
NoPlat 4M		-5.1	
upper Wellington Fm, Waurika, OK	284.6		-8.6 (±0.6)
WAR 1B.1		-8.3	
WAR 2B.1		-8.2	
WAR 2B.2		-9.3	
WAR 4B.1		-7.4	
WAR 4B.2		-7.7	
WAR 4C.1		-9.6	
WAR 4C.2		-9.3	
WAR 4C.3		-9.1	
basal Petrolia Fm, upper Parkeys Oil Patch, nc- TX	284.2		-6.4 (±1.0)
POP 1E		-7.7	
POP 1C		-6.6	
POP 1G		-8.7	
POP 2D		-5.1	
POP 4GA		-5.4	
POP 4GB		-5.5	
POP 4H		-5.9	
upper Wellington Fm, OK	283.8		-8.7 (±0.1)
OK 2.1.1		-8.7	
OK 2.1.2		-8.8	
OK 2.3.1		-8.6	
OK 2.3.2		-8.6	

Table S1. continued

Samples	Age[1] (Ma)	$\delta^{13}C_{ped\ carb}$ measured	$\delta^{13}C_{ped\ carb}$ Avg. (±2 s.e.)
middle Petrolia Fm, Amphitheater, nc- TX	283.4		-9.5 (±0.8)
PAM 2D		-10.0	
PAM 2DR		-9.8	
PAM1C		-10.5	
PAM1C2		-10.4	
PAM 2E		-10.8	
PAM 2F		-10.6	
PAM 3C-1		-9.4	
PAM 3C-2		-8.9	
PAM 1O		-8.2	
PAW1		-6.9	
upper Petrolia Fm, Hentz stratotype, nc- TX	282.2		-7.3 (±0.2)
PSTL 2E		-7.3	
PSTL 2E		-7.4	
PSTL 3G2		-7.3	
PSTL 3G3		-7.2	
PSTL 3G5		-7.8	
PSTL 3H		-7.1	
PSTL 3H		-7.0	
uppermost Petrolia Fm, Castle Hollow, nc- TX	281.9		-5.1 (±0.5)
CPU 12		-5.4	
CPU 12		-5.2	
CPU 9B-1		-4.7	
CPU 9B-2		-4.5	
CPU 8		-5.9	
Organ Rock, se-UT	281.8		-2.5 (±0.1)
OR2-1		-2.5	
OR2-2		-2.6	
middle Waggoner Ranch Fm, Franklin Bend, nc- TX	280.9		-5.8 (±1.0)
WFBU 1D		-4.8	
WFBU10E-1		-3.8	
WFBU10E2		-4.9	
WFBU4D-1		-4.8	
WFBU4D-2		-6.2	
WFBU4E-1		-6.7	
WFBU4E-2		-6.9	
WFBU4D-3		-7.8	

Table S1. continued

Samples	Age[1] (Ma)	$\delta^{13}C_{ped\ carb}$ measured	$\delta^{13}C_{ped\ carb}$ Avg. (±2 s.e.)
Upper Waggoner Ranch Fm, Mitchell Creek, nc-TX	280.2		-5.4 (±0.5)
MCLRUS		-4.6	
MC0		-4.6	
MC 25		-5.4	
MC 28B		-5.5	
WCB1A		-5.7	
WCB 2-1		-5.7	
WCB5		-6.0	
WCB 7		-5.9	
WCB 30		-7.9	
WCB 33		-5.2	
WCB 36		-4.6	
WCB 38		-4.8	
WCB 40		-4.8	
WCB44		-5.3	
WCB 50		-5.2	
uppermost Garber Fm, OK	280.1		-6.0 (±0.4)
OK 3.1.1		-6.4	
OK 3.3.1		-5.7	
OK 3.3.2		-5.8	
Leuders Fm, nc-TX	279.8		-4.5 (±0.7)
TWA		-5.4	
TWB		-5.3	
LL1		-5.0	
LL2		-5.2	
LL3		-5.3	
LL-4		-5.2	
L-99-3		-2.8	
L-99-2		-3.8	
L-99-2R		-3.6	
L-99-4		-1.4	
MLEU1		-4.1	
ULEU 1		-5.8	
ULEU 2		-6.1	
basal Clear Fork Gp, Craddock Ranch, nc-TX	279.3		-4.3 (±1.1)
CFC 2E-1		-3.2	
CFC 2F		-6.1	
CFC 3-1		-3.8	
CFC 3D-1		-4.0	
CFC 1G-1		-4.1	

Table S1. continued

Samples	Age[1] (Ma)	$\delta^{13}C_{ped\ carb}$ measured	$\delta^{13}C_{ped\ carb}$ Avg. (±2 s.e.)
Arroyo Fm, Clear Fork Gp, Hog Creek, nc-TX	278.9		-5.0 (±0.6)
HC2(A)		-6.4	
HC2(B)		-5.3	
HC8A(1)		-4.6	
HC8A(2)		-4.7	
HC9A		-4.1	
HC11A		-5.0	
basal Vail Fm, Clear Fork Gp, Hog Creek, nc-TX	278.1		-5.1 (±0.9)
CF-1A-1		-4.9	
CF-1A-2		-5.1	
CF-1A-R		-5.0	
CF-1B		-4.0	
99-CF-2		-6.5	
Vail Fm, Clear Fork Gp, Wichita River, nc-TX	277.1		-4.5 (±0.8)
WRVF8		-3.4	
WRVF12		-4.0	
WRVF20		-4.8	
WRVF22		-4.7	
WRVF26		-5.6	
Choza Fm, Clear Fork Gp, Montgomery Ranch, nc-TX	274.4		-4.8 (±0.2)
MG3A		-4.6	
MG11A		-4.9	
MG5		-4.8	
MG 16A		-5.1	

[1]Ages of localities based on stratigraphic age model developed in this study and calibrated to the Geologic Time-Scale 2004 (*S11*).

Table S2. Fossil organic matter $\delta^{13}C$ values used for paleo-pCO_2 reconstruction.

Formation & Locality	Age[1] (Ma)	Sample ID	Material Analyzed	$\delta^{13}C_{org}$ [2] measured	$\delta^{13}C_{org}$ [3] Fm Avg.	$\delta^{13}C_{org}$ ±2 X std. err. (count)
Markley Formation, nc-Texas:					-22.8	±0.3 (33)
Brannon Mine	301.3	A3	carbonized wood	-22.7		
Newcastle & Coal Mountain	300.8	A4	compression plant	-21.0		
Newcastle	300.8	A17	bulk organic matter			
Bloodworth	300.3	A1	compression plant	-23.7		
Bloodworth, Cooper	300.3	WAD 1	compression plant	-23.4		
Bloodworth, Cooper	300.3	WAD 1R	compression plant	-23.6		
Bloodworth, Cooper	300.3	WAD 2	compression plant	-22.7		
Bloodworth, Cooper	300.3	WAD 2R	compression plant	-22.8		
Cooper	300.3	WAD 5	compression plant	-24.3		
Cooper	300.3	WAD6R	compression plant	-22.3		
Cooper	300.3	WAD6	compression plant	-23.0		
Cooper	300.3	A5	bulk organic matter	-23.4		
Cooper upper beds	300.3	A6	compression plant	-23.8		
Cooper lower shale	300.3	A7	bulk organic matter	-23.2		
Gillespies	300.3	A8	compression plant	-21.3		
Loving West	300.3	A9	compression plant	-22.4		
Bloodworth, Cooper	300.3	A10	coal	-23.8		
Lycopod	300.3	A11	compression plant	-22.1		
Lycopod B	300.3	A12	coal	-23.9		
Bloodworth Bed 12	300.3	A13	compression plant	-22.7		
Williamson Dr.	300.3	A16	charcoal	-21.2		
Williamson Dr	300.3	WAD 3	compression plant	-22.3		
Williamson Dr	300.3	WAD 4	compression plant	-22.9		
Williamson Dr	300.3	WAD 4R	compression plant	-23.5		
Williamson Dr	300.3	A16	charcoal	-21.8		
Williamson Dr	300.3	A15	charcoal	-22.4		
Voyles Coal	298.6	A14	charcoal	-23.5		
Malone Ranch &Antelope	298.5	A2	compression plant	-22.9		
Walker	298.5	MBW1A	compression plant	-22.7		
Walker	298.5	MBW1B	compression plant	-23.0		
Walker	298.2	WAD8	compression plant	-22.2		
Walker	298.3	WAD 7	compression plant	-22.5		

Table S2. Continued

Formation & Locality	Age[1] (Ma)	Sample ID	Material Analyzed	$\delta^{13}C_{org}$[2] measured	$\delta^{13}C_{org}$[3] Fm Avg.	$\delta^{13}C_{org}$ ±2 X std. err. (count)
Archer City Formation, nc-Texas:					-22.1	±1.1 (10)
Andrews	297.1	D2	compression plant	-19.8		
Andrews	296.1	AC24	paleosol organic matter	-21.7		
Sanzenbacher #1	296.1	D5	fossil seed pod	-20.6		
Sanzenbacher #2	296.1	D6	carbonized stem	-20.8		
Kola Switch Lower Beds	295.8	D3	carbonized stem	-21.9		
Kola Switch	295.8	D4	carbonized stem	-21.3		
Kola Switch	295.8	WAD10	compression plant	-24.6		
Kola Switch	295.8	WAD10R	compression plant	-24.5		
Kola Switch	295.8	WAD11	compression plant	-23.4		
Kola Switch	295.8	WAD11R	compression plant	-23.5		
Bonebed #3	295.1	D1	carbonized wood	-20.2		
Wellington Formation, Oklahoma:					-20.8	±0.9 (2)
Perry #7	296.0	C4-OK	coal	-20.2		
Perry	296.0	C5-OK	carbonized wood	-21.4		
Nocona Formation, NC Texas					-20.8	±1.1 (6)
Cooper Mine	292.0	D7	carbonized stem	-19.2		
Rattlesnake Canyon	288.2	D9	carbonized stem	-22.5		
Rattlesnake Canyon	288.2	D10	carbonized stem	-22.6		
Rattlesnake Canyon South	288.2	D27	charcoal	-20.2		
South of Black Flats	285.9	D11	carbonized stem	-19.7		
South of Black Flats	285.9	D12	carbonized stem	-20.4		
Abo Formation, New Mexico					-22.0	±0.7 (9)
Socorro to Las Cruces vicinity	289.6	D41	charcoal	-23.8		
Socorro to Las Cruces vicinity	289.6	B2	conifer stem	-21.2		
Socorro to Las Cruces vicinity	289.6	B7	carbonized wood	-22.5		
Socorro to Las Cruces vicinity	288.7	B4	carbonized wood	-20.9		
Socorro to Las Cruces vicinity	288.7	B6	bulk organic matter	-21.5		
Socorro to Las Cruces vicinity	285.9	B8	compression plant	-21.9		
Socorro to Las Cruces vicinity	286.8	B1	charcoal	-23.4		
Socorro to Las Cruces vicinity	288.7	B5	carbonized wood	-20.6		

Table S2. Continued

Formation & Locality	Age[1] (Ma)	Sample ID	Material Analyzed	$\delta^{13}C_{org}$ [2] measured	$\delta^{13}C_{org}$ [3] Fm Avg.	$\delta^{13}C_{org}$ ±2 X std. err. (count)
Socorro to Las Cruces vicinity	286.8	B3	carbonatized cone	-21.5		
Petrolia Fm, nc-TX					-21.1	±0.5 (23)
Parkey's Oil Patch	284.2	POP-1	carbonized stem	-20.5		
Parkey's Oil Patch	284.2	D8	carbonized stem	-19.5		
Godwin Creek	284.1	D21	carbonized stem	-19.0		
Fire in the Swamp	284.1	D28	charcoal	-21.1		
South of Fishhook Ridge	284.1	D30	charcoal	-23.2		
Parkey's Oil Patch	284.1	POP-2	compression plant	*-20.4*		
Parkey's Oil Patch	284.1	D24	charcoal	-20.0		
Wallace Pocket	283.9	D32	charcoal	-21.2		
Spider Hollow	283.8	D31	charcoal	-19.8		
Emily Irish	283.7	D85	charcoal	-19.9		
Red Hollow	283.4	RH-1	charcoal	-20.9		
Red Hollow	283.4	D25	charcoal	-20.6		
Meteor Tank	283.3	D22	charcoal	-20.4		
Meteor Tank	283.3	D23	charcoal	-22.0		
White's Crossing Cowan 's	282.5	D33	charcoal	-22.2		
Haycamp Gigantopterid	282.3	D29	charcoal	-20.1		
Castle Hollow	282.0	D15	carbonized seed	-19.8		
Castle Hollow	282.0	D17	carbonized stem	-23.0		
Fulda East Road	282.0	D18	carbonized stem	-21.9		
Fulda East Road	282.0	D19	carbonized stem	-21.4		
Fulda East Road	282.0	D20	carbonized stem	-23.2		
Burnt Stump 1991-28	282.0	BS-1	charcoal	-23.0		
Burnt Stump Bottom Beds	282.0	D14	charcoal	-22.3		
Lower Waggoner Ranch Fm, nc-TX					-21.5	±1.3 (5)
Fulda Ford Cowan Ranch	281.8	D26	charcoal	-22.6		
Boggy Creek	281.6	D71	charcoal	-22.4		
Farmer Tank	281.2	D37	charcoal	-20.3		
Taint A (Franklin Bend Vicinity)	280.9	D76	charcoal	-19.2		
Cowan	281.3	D34	charcoal	-22.9		

Table S2. Continued

Formation & Locality	Age[1] (Ma)	Sample ID	Material Analyzed	$\delta^{13}C_{org}$[2] measured	$\delta^{13}C_{org}$[3] Fm Avg.	$\delta^{13}C_{org}$ ±2 X std. err. (count)
Upper Waggoner Ranch Fm, nc-TX					-20.9	±0.5 (22)
Stout - Middle unit	280.7	D78	carbonized stem	-22.1		
Stout	280.7	D79	charcoal	-22.5		
Waggoner New Fence Line	280.4	LWG-1	charcoal	-19.6		
Waggoner New Fence Line	280.4	D77	charcoal	-19.9		
S.S. below Wattia II	280.4	D74	charcoal	-22.4		
Eurypterid locality 94-26A	280.3	D35	charcoal	-20.4		
Wattia II	280.3	WII-1	charcoal	-19.3		
Wattia II	280.3	D73	charcoal	-19.7		
Wattia II	280.3	D72	charcoal	-20.1		
Eurypterid locality	280.3	ER-1	charcoal	-21.7		
E. of 283 N. of Wichita River	280.3	D38	charcoal	-21.0		
Old Spillway Lake Kemp	280.3	D39	charcoal	-19.3		
Lake Kemp Dam	280.1	D36	charcoal	-19.5		
Mitchell Creek West Site C	280.1	D80	charcoal	-19.2		
Mitchell Creek	280.1	42138-1	cuticle	-22.2		
Mitchell Creek	280.1	42138-2	cuticle	-22.5		
Mitchell Creek	280.1	MC-1	charcoal	-21.2		
Lake Kemp Dam	280.1	D40	charcoal	-21.6		
Mitchell Creek Chert A	280.1	D81	coal	-22.0		
Mitchell Creek Flats	280.1	D82	charcoal	-22.7		
Mitchell Creek	280.1	D83	charcoal	-19.9		
Cutbank	280.1	WCB-1	paleosol organic matter	-19.7		
Cutbank	280.1	QCB-2	paleosol organic matter	-19.9		
Cutbank	280.1	WCB-3	paleosol organic matter	-20.2		
Leuders Fm, nc-TX					-20.8	±0.4 (7)
Wattia I Moonshine	279.9	WI-1	charcoal	-20.5		
Little Moonshine	279.9	D69	charcoal	-21.0		
Little Moonshine	279.9	D70	charcoal	-20.7		
Little Moonshine	279.9	D75	charcoal	-20.7		
Wattia I	279.8	D16	carbonized stem	-22.1		
Wattia I	279.8	D65	compression plant	-20.3		
Mitchell Creek Flats	279.7	MC-2	charcoal	-20.4		

Table S2. Continued

Formation & Locality	Age[1] (Ma)	Sample ID	Material Analyzed	$\delta^{13}C_{org}$ [2] measured	$\delta^{13}C_{org}$ [3] Fm Avg.	$\delta^{13}C_{org}$ ±2 X std. err. (count)
Arroyo Fm, Clear Fork Gp, nc-TX					-21.9	±0.6 (9)
Grayback Oil Field I	279.5	D68	charcoal	-21.0		
Grayback Oil Field I	279.5	D67	charcoal	-20.6		
Pony Creek	279.5	D61	Trigonocarpus plant	-23.1		
Pony Creek	279.5	D62	charcoal	-23.4		
Harmel Quarry main site	279.5	D63	charcoal	-21.7		
Craddock	279.3	CR-1	charcoal	-22.6		
Craddock	279.3	D66	charcoal	-21.8		
NRU 3533 6881'-6890'	279.1	D51	charcoal	-21.2		
HogCreek Pond	279.0	HC8	paleosol organic matter	-21.5		
HogCreek Pond	279.0	D64	charcoal	-21.5		
Vail Fm, Clear Fork Gp, nc-TX					-21.2	±0.9 (9)
NRU 207 6583'	277.1	D43	charcoal	-21.8		
NRU 3533 6625.5'-6636'	278.0	D44	charcoal	-20.9		
NRU 207 6407'-6408'	278.5	D46	charcoal	-21.0		
NRU 207 6619'	278.0	D47	compression plant	-22.7		
NRU 3533 6682'-6685'	278.6	D48	charcoal	-19.2		
NRU 207 6644'	278.5	D49	charcoal	-19.8		
NRU 3533 6691'-6691.5'	278.6	D50	charcoal	-21.2		
NRU 3522 6606'-6609'	278.0	D52	charcoal	-23.4		
NRU 3522 6712.3'-6712.8'	278.5	D53	charcoal	-20.4		
Wichita River outcrop	278.8	WRVF7	paleosol organic matter	-22.6		
Wichita River outcrop	278.8	WRVF23	paleosol organic matter	-21.8		
Hennessy Fm, Oklahoma					-19.7	±0.1 (2)
East Manitou Roadcut	277.4	C2	carbonized wood	-19.6		
East Manitou Roadcut	277.4	HCF-1	compression plant	-19.8		
Choza Fm, Clear Fork Gp, nc-TX					-21.1	±0.6 (2)
NRU 207 5960.7'	272.6	D42	charcoal	-21.7		
NRU 207 6243'-6244'	274.3	D45	charcoal	-20.5		
Montgomery Ranch	274.3	MG5	paleosol organic matter	-22.2		
Montgomery Ranch	273.3	MG7	paleosol organic matter	-21.6		

Table S2. Continued

Formation & Locality	Age[1] (Ma)	Sample ID	Material Analyzed	$\delta^{13}C_{org}$[2] measured	$\delta^{13}C_{org}$[3] Fm Avg.	$\delta^{13}C_{org}$ ±2 X std. err. (count)
San Angelo & Blaine Fms, nc-TX						
Buzzard Peak	272.3	D54	charcoal	-22.0	-21.1	±0.6 (14)
San AngeløBlaine contact	272.0	SABC-1	charcoal	-21.1		
San AngeløBlaine contact	272.0	SABC-2	charcoal	-20.5		
San AngeløBlaine contact	272.0	SABC-3	charcoal	-21.4		
East Taylor Pasture	272.5	ETP-1	charcoal	-19.5		
East Taylor Pasture	272.5	D60	charcoal	-19.7		
Log Jam	272.5	D56	charcoal	-20.7		
Pyron Prospect	272.3	D57	charcoal	-21.6		
Brazos-Wichita Mine	272.4	D58	charcoal	-20.4		
Snake Den Shooting Range	272.6	D59	charcoal	-20.8		
Devil's Canyon	272.2	42104	cuticle	-23.0		
Devil's Canyon	272.3	42104R	cuticle	-22.8		
Devil's Canyon	272.3	42105	cuticle	-22.3		
South Ash Pasture	272.3	D55	charcoal	-20.2		

[1]Ages of localities based on stratigraphic age model developed in this study and calibrated to the Geologic Time-Scale 2004 (S11).

[2]Values reflect average of 3 sample replicates.

[3]Average, standard error, and count values do not include paleosol organic matter data.

Table S3. Input parameters for paleobarometer estimates (symbols on Fig. 1C) and Monte Carlo modeling of paleo-atmospheric pCO_2.

Formation	Age[1]	Paleosol	$\delta^{13}C_{ped\ carb}$	$\delta^{13}C_{plant}$[2]	$\delta^{13}C_{ATM}$[3]	$\delta^{13}C_{oil\text{-}respired\ CO2}$[4]		Temp.	Total Soil CO_2	
	(Ma)		Avg. (±2 s.e.)	Avg. (±2 s.e.)	Avg. (±2 s.e.)	Avg.	Range	(± 3°C)	Best (ppmv)	Range (ppmv)
Honaker Trail Fm, UT	300.3	sandy Calcisols	-3.4 (±0.6)	-21.0 (±1.0)	-2.5 (±1.0)	-12.1	-13.0 to –11.2	27	2500	1000 - 3000
Hermit Shale Fm, Kohl's Ranch, AZ	300.0	Calcisols	-4.2 (±1.1)	-21.0 (±1.0)	-2.5 (±1.0)	-13.2	-14.6 to –11.8	24	3000	2000 - 5000
Bursum Fm, Socorro, NM	299.8	Calcisols	-6.1 (±0.3)	-21.5 (±1.1)	-3.0 (±1.1)	-14.9	-15.6 to –14.2	25	5000	2000 - 5000
upper Halgaito Fm, AZ	298.6	Silty Calcisols	-4.0 (±0.2)	-21.0 (±0.8)	-2.5 (±0.8)	-12.5	-13.1 to –11.9	30	3000	1500 - 4000
Hermit Shale Fm, Flagstaff, AZ	297.7	muddy Calcisols	-5.9 (±0.6)	-21.0 (±0.8)	-2.5 (±0.8)	-14.4	-15.4 to –13.4	28	3000	2000 - 5000
middle Archer City Fm, stratotype (SS5), nc-TX	296.0	calcic Vertisols, Aridisols	-9.3 (±2.1)	-21.8 (±0.5)	-3.3 (±0.5)	-17.2	-19.6 to –14.7	33	5500	3200 - 7500
upper Archer City Fm bonebed (SS8), nc-TX	295.1	carb-Vertisols, Aridisols, Alfisols	-9.4 (±1.0)	-21.8 (±0.5)	-3.3 (±0.5)	-17.0	-18.4 to-15.6	36	7500	6000 - 8000
basal Nocona Fm, coprolite bonebed, nc-TX	292.4	calcic Vertisols	-9.5 (±1.0)	-21.8 (±1.1)	-3.3 (±1.1)	-17.1	-18.4 to –15.7	36	6000	4000 - 8000
middle Nocona Fm, nc-TX	290.0	calcic Vertisols	-8.6 (±0.8)	-21.8 (±1.1)	-3.3 (±1.1)	-16.3	-17.4 to –15.2	35	6000	4000 - 8000
Abo Fm, Socorro to Las Cruces, NM	285.2	calcic Vertisols	-5.6 (±0.6)	-21.9 (±0.7)	-3.4 (±0.7)	-13.6	-14.6 to –12.7	32	6000	4000 - 8000
upper Hermit Shale Fm, Nash Pt & Fossil Springs, AZ	285.1	Vertisols, histosols	-5.1 (±1.1)	-21.0 (±1.0)	-2.5 (±1.0)	-12.8	-14.2 to –11.4	35	7000	5000 - 8000
Cedar Mesa Fm, se-UT	285.0	sandy calcisols	-3.2 (±0.6)	-21.0 (±1.0)	-2.5 (±1.0)	-11.3	-12.3 to –10.3	32	2000	1000 - 3000
uppermost Nocona Fm, lower Parkey's Oil Patch, nc- TX	285.0	calcicVertisols, Aridisols, Alfisols	-5.6 (±0.9)	-21.8 (±1.1)	-3.3 (±1.1)	-14.2	-15.4 to –12.9	28	7500	6000 - 9000
Wellington Fm, Waurika, OK	284.6	Vertisols, histosols	-8.6 (±1.0)	-22.0 (±1.0)	-3.5 (±1.0)	-16.7	-18.0 to –15.3	32	7000	5000 – 8000

Table S3. continued

Formation	Age[1] (Ma)	Paleosol	$\delta^{13}C_{ped\ carb}$ Avg. (±2 s.e.)	$\delta^{13}C_{plant}$[2] Avg. (±2 s.e.)	$\delta^{13}C_{ATM}$[3] Avg. (±2 s.e.)	$\delta^{13}C_{oil\text{-}respired\ CO2}$[4] Avg.	Range	Temp. (± 3°C)	Total Soil CO_2 Best (ppmv)	Range (ppmv)
basal Petrolia Fm, upper Parkey's Oil Patch, nc- TX	284.2	Aridisols	-6.4 (±1.0)	-21.5 (±0.7)	-3.0 (±0.7)	-14.0	-15.3 to –12.6	36	4000	2500 - 5000
Wellington Fm, OK	283.8	calcic Vertisols, Aridisols	-8.7 (±0.1)	-22.0 (±1.0)	-3.5 (±1.0)	-16.8	-17.3 to –16.4	31	5500	2500 - 7500
middle Petrolia Fm, Amphitheater, nc- TX	283.4	calcic Vertisols, Aridisols	-9.5 (±0.8)	-22.6 (±0.6)	-4.1 (±0.6)	-17.7	-18.8 to –16.6	31	5500	3200 - 7500
upper Petrolia Fm, Hentz stratotype, nc- TX	282.2	calcic Alfisols, Aridisols	-7.3 (±0.2)	-22.6 (±0.6)	-4.1 (±0.6)	-15.4	-16.0 to –14.9	31	7000	5000 - 8000
uppermost Petrolia Fm, Castle Hollow, nc- TX	281.9	Aridisols	-5.1 (±0.5)	-22.6 (±0.6)	-4.1 (±0.6)	-13.0	-13.9 to –12.2	33	4000	2500 - 5000
Organ Rock, se-UT	281.8	muddy Calcisols	-2.5 (±0.1)	-21.0 (±1.0)	-2.5 (±1.0)	-10.8	-11.3 to –10.3	30	3000	2000 - 4000
middle Waggoner Ranch Fm, Franklin Bend, nc- TX	280.9	calcic Vertisols, Aridisols	-5.8 (±1.0)	-21.7 (±0.5)	-3.2 (±0.5)	-13.5	-14.8 to –12.1	35	5500	3200 - 7500
Upper Waggoner Ranch Fm, Mitchell Creek, nc-TX	280.2	calcic Vertisols, Aridisols	-5.4 (±0.5)	-21.7 (±0.5)	-3.2 (±0.5)	-13.7	-14.5 to –12.9	30	5500	3200 - 7500
uppermost Garber Fm, OK	280.1	calcic Vertisols, Aridisols	-6.0 (0.4)	-22.4 (±0.5)	-3.9 (±0.5)	-14.3	-15.0 to –13.6	30	5500	2500 - 7500
Leuders Fm, nc-TX	279.8	calcic Vertisols, Aridisols	-4.5 (0.7)	-21.5 (±0.7)	-3.0(±0.7)	-12.8	-13.9 to –11.7	30	5500	3200 – 7500
basal Clear Fork Gp, Craddock Ranch, nc-TX	279.3	calcic Vertisols, Aridisols	-4.3 (±1.1)	-22.2 (±0.6)	-3.7 (±0.6)	-12.6	-14.1 to –11.1	30	5500	3200 - 7500
Arroyo Fm, Clear Fork Gp, Hog Creek, nc-TX	278.9	calcic Vertisols, Aridisols	-5.0 (±0.6)	-22.9 (±0.6)	-4.4 (±0.6)	-13.4	-14.4 to –12.4	29	5500	3200 - 7500
basal Vail Fm, Clear Fork Gp, Hog Creek, nc-TX	278.1	calcic Vertisols, Aridisols	-5.1 (±0.9)	-22.9 (±0.6)	-4.4 (±0.6)	-13.5	-14.8 to –12.3	29	6500	3200 - 7500
Vail Fm, Clear Fork Gp, Wichita River, nc-TX	277.1	calcic Vertisols, Aridisols	-4.5 (±0.8)	-22.9 (±0.6)	-4.4 (±0.6)	-12.9	-14.0 to –11.8	29	5500	3200 - 7500
Choza Fm, Clear Fork Gp, Montgomery Ranch, nc-TX	274.4	carb-Vertisols, Aridisols	-4.8 (±0.2)	-22.9 (±0.6)	-4.4 (±0.6)	-13.4	-13.9 to –12.8	28	5500	3200 - 7500

Table S3. continued

[1]Ages of localities based on stratigraphic age model developed in this study and calibrated to the Geologic Time-Scale 2004 (*S11*).

[2]Input values adjusted by –0.7 to –1‰ from measured values to account for ^{13}C enrichment during bacterial decay and/or thermal maturation as suggested by C/N ratios and thermal maturity of materials.

[3]calculated using $\Delta^{13}C = \delta^{13}C_{atm} - \delta^{13}C_{org}$ of 18.5‰

[4]calculated as $(\delta^{13}C_{carb} + 1000)/\exp((11.98 - 0.12*temp)/1000)-1000$

Table S4. Monte Carlo modeling of paleo-pCO_2: Modeled CO_2 contents.

Age (Ma)	Modeled pCO_2 (best, ppmv)	Modeled pCO_2 (min., ppmv)	Modeled pCO_2 (max., ppmv)
300.2	1103.1	353.0	1683.3
299.9	1045.8	277.9	1653.7
299.7	997.0	219.5	1624.6
299.4	951.6	168.2	1595.0
299.1	902.9	111.7	1564.0
298.8	844.1	37.7	1530.5
298.6	772.7	-38.1	1493.8
298.3	691.9	-112.1	1454.0
298.0	605.8	-215.4	1411.2
297.8	518.0	-329.4	1365.5
297.5	432.6	-451.7	1316.9
297.2	353.3	-558.8	1265.5
296.9	284.2	-643.1	1211.5
296.7	228.9	-697.0	1154.8
296.4	191.4	-712.7	1095.6
296.1	175.0	-684.2	1034.3
295.9	175.1	-624.2	974.4
295.6	181.7	-558.3	921.7
296.3	187.0	-506.7	880.8
295.0	190.0	-471.1	851.0
294.8	190.8	-449.4	831.0
294.5	189.9	-439.5	819.4
294.2	187.6	-439.5	814.6
294.0	184.2	-447.1	815.4
295.6	179.9	-460.3	820.2
293.4	175.2	-477.1	827.6
293.1	170.4	-495.4	836.1
292.9	165.7	-513.0	844.4
292.6	161.5	-528.0	851.0
292.3	158.1	-538.2	854.5
292.0	157.1	-541.9	856.0
291.8	161.7	-537.5	860.9
291.5	175.7	-523.7	875.0
291.2	202.6	-498.9	904.1
291.0	246.0	-461.9	954.0
290.7	309.7	-411.3	1030.6
290.4	397.1	-345.5	1139.7
290.1	512.0	-263.1	1287.1
289.9	657.7	-162.9	1478.3
289.6	833.0	-46.0	1712.0
289.3	1031.5	84.0	1979.1
289.1	1246.5	223.0	2270.1
288.8	1471.3	367.2	2575.5
288.5	1699.2	512.6	2885.9
288.2	1923.5	655.4	3191.6
288.0	2117.5	791.6	3383.3
287.7	2164.4	817.3	3501.5
287.4	2307.6	928.6	3686.6
287.2	2450.5	1021.7	3879.3

Table S4. continued

Age (Ma)	Modeled pCO_2 (best, ppmv)	Modeled pCO_2 (min., ppmv)	Modeled pCO_2 (max., ppmv)
286.9	2556.2	1092.5	4019.9
286.6	2618.1	1137.1	4099.0
286.3	2629.5	1151.8	4107.2
286.1	2583.6	1132.4	4034.8
285.8	2473.9	1075.2	3872.5
285.6	2293.5	976.3	3610.8
285.4	2035.9	831.6	3240.1
285.2	1895.3	738.4	3052.1
285.0	1700.0	529.7	2496.9
284.6	1513.3	353.1	1983.6
284.2	1240.0	204.1	1540.7
283.9	640.4	85.2	1195.7
283.8	513.9	31.3	996.5
283.3	516.4	68.6	964.2
283.1	651.4	208.2	1094.5
282.8	889.5	426.4	1352.6
282.5	1187.2	684.0	1690.4
282.3	1500.7	941.7	2059.6
282.0	1786.2	1160.2	2412.1
281.9	1999.8	1301.8	2697.8
281.9	2121.1	1355.2	2887.1
281.8	2173.4	1347.8	2998.9
280.9	2184.3	1310.9	3057.6
280.6	2181.5	1275.8	3087.3
280.4	2191.7	1269.9	3113.5
280.1	2234.1	1297.6	3170.6
279.8	2324.1	1355.2	3293.1
279.5	2463.5	1442.6	3484.4
279.4	2650.8	1563.8	3737.8
279.2	2853.8	1704.3	4003.3
279.0	3009.4	1828.8	4190.0
278.8	3102.0	1916.4	4287.6
278.7	3135.6	1960.6	4310.7
278.5	3120.8	1965.9	4275.7
278.3	3068.3	1937.3	4199.2
278.1	2998.0	1886.1	4110.0
278.0	2991.9	1865.7	4118.1
277.8	3090.3	1906.1	4274.6
277.6	3234.3	1976.4	4492.3
277.4	3362.5	2043.8	4681.3
277.2	3457.1	2098.5	4815.7
277.1	3521.0	2141.7	4900.4
276.9	3557.3	2174.3	4940.3
276.7	3569.0	2197.7	4940.4
276.5	3559.3	2213.0	4905.7
274.9	3531.2	2221.3	4841.2
274.4	3487.8	2223.8	4751.8
274.1	3432.2	2221.7	4642.7
273.8	3367.5	2216.2	4518.7
273.6	3296.6	2208.3	4384.9
273.3	3222.8	2199.4	4246.3

Table S5. Compilation of published brachiopod $\delta^{18}O$ and detrended (± std. error) values, and corresponding paleotemperature estimates.

Age[1] (Ma)	Count (n)	Mean $\delta^{18}O$	±2 std. err.	Source[2]	Mean $\delta^{18}O$ detrended	±2 std. err.	$\delta^{18}O_{water}$ ‰	Est. Temp.[3] Best (°C)	Est. Temp.[3] Range (°C)
303.5	33	-2.6	0.4	1, 4	0.7	0.4	0 to 0.5	10.7 to 13.0	9.0 to 14.8
302.5	84	-2.4	0.2	1, 4	0.9	0.2	0 to 0.5	10.1 to 12.3	9.0 to 13.4
301.5	86	-2.8	0.1	1, 4	0.5	0.1	0 to 0.5	11.7 to 13.9	11.0 to 14.6
300.5	30	-2.6	0.6	1, 2, 3, 4	0.7	0.6	0 to 0.5	10.8 to13.0	8.2 to 15.7
299.5	9	-2.7	0.3	1, 4	0.6	0.3	0 to 0.5	11.5 to 13.7	10.1 to 15.2
298.5	8	-1.3	0.6	1, 5	1.9	0.6	0 to 1.5	5.6 to12.1	3 to 14.9
297.5	15	-1.8	1.1	1, 5	1.4	1.1	0 to 1.5	7.8 to 14.4	3.1 to 19.6
296.5	5	-3.2	1.7	1, 5	0.1	1.4	0 to 1.0	13.3 to 17.9	7.3 to 24.5
295.5	6	-2.9	1.7	1, 5	0.2	1.5	0 to 1.0	13.0 to 17.6	6.3 to 25.0
294.5	2	-2.1	1.4	1, 5	1.1	1.4	0 to 1.5	9.2 to 16.0	3.3 to 22.6
293.5	4	-2.7	2.4	1, 5	1.8	0.3	0 to 1.5	6.2 to 12.8	5.0 to 14.0
290.3	3	-4.2	2.4	1, 5	-1.1	2.4	0 to -0.5	19.3 to 16.9	6.1 to 31.5
286.0	2	-5.1	1.0	1	-2.3	0.7	0 to -0.5	22.7 to 25.1	19.2 to 28.7
287.5	2	-2.9	0.9	1, 5	-0.6	0.2	0 to -0.5	14.6 to 16.9	13.8 to 17.8
285.0	19	-4.1	0.6	1, 2	-1.2	0.6	0	19.4	16.7 to 22.1
284.2	6	-5.5	1.3	1	-2.6	1.6	0	26.2	18.5 to 34.3
283.4	3	-2.3	0.5	5	0.8	0.5	0 to 1.0	10.5 to 15.0	8.5 to 17.1
280.5	11	-3.5	0.2	1, 5	-0.6	0.2	0	16.9	15.9 to 17.9
278.5	3	-6.6	0.3	1	-3.7	0.3	0 to -0.5	29.5 to 32.1	28.1 to 33.5
276.0	3	-2.9	0.1	5	-0.5	0.3	0	16.1	14.7 to 17.6
275.5	3	-6.2	1.5	1	-3.4	1.5	0 to -0.5	28.1 to 30.7	20.7 to 38.6
274.5	8	-2.9	1.5	1, 5	-0.1	1.5	0 to -0.5	14.2 to 16.5	7.6 to 23.7
272.5	51	-2.0	0.5	1, 2	0.7	0.5	0 to 1.0	10.6 to 15.2	8.4 to17.5
271.5	14	-1.6	1.1	1, 3	1.1	1.1	0 to 1.5	8.9 to 15.6	4.2 to 20.8
270.5	14	-3.1	0.5	1, 3, 5	-0.3	0.5	0 to 1.0	15.3 to 20.0	13.0 to 22.3
269.5	6	-3.3	1.2	1	-0.6	1.2	0 to 1.0	16.6 to 21.4	11.0 to 27.5
268.5	16	-4.4	0.8	1, 5	-1.7	0.8	0	22.0	18.0 to 26.1
267.5	5	-2.4	1.0	1, 5	0.3	1.0	0	12.5	8.0 to 17.1
266.5	4	-2.4	0.8	1, 5	0.3	0.8	0	12.5	8.9 to 16.3
265.0	4	-4.6	0.4	1	-1.9	0.4	0 to -0.5	20.6 to 23.0	18.6 to 25.1

[1]Values adjusted to the Geologic Time-Scale 2004 (*S11*) and binned into 1 to 3 m.y. windows; age noted is mid-point of range.

[2]Data from (1) *S12* - including data from *S13*-S17; (2) *S18*; (3) *S19, S20*; (4) *S21*; (5) *S22* ('best-preserved' samples with exception of two in *M. biselli – S. whitei* due to paucity of data in this interval).

[3]Note that paleotemperature estimates on Figures 2B and 3C are shown as temperature anomalies (relative to 17.5°C) calculated from a 3-pt weighted running average (± 2 std. err.) through binned detrended $\delta^{18}O_{brach}$.

Table S6. Stratigraphic and temporal abundance patterns of fossil plants in north-central Texas (Eastern Shelf).

Age[1] (Ma)	Formation	Field Locality	Conifers[2]	Peltasperms[2, 3]	Marattialean[2, 4] Ferns	Medullosan[2, 5] Pteridosperms
301.9	Markley	*Turnbow*	0	0	5	5
301.7	Markley	*Turnbow kaolinite*	3	0	0	1
301.3	Markley	*Cooper kaolinite*	1	0	0	1
301.2	Markley	*Bloodworth & Cooper*	0	0	5	5
300.4	Markley	*Walker, Williamson Drive, Gillespie & Lycopod B*	0	0	5	5
300.0	Markley	*Voyles*	1	0	5	5
299.2	Markley	*281 Roadcut kaolinite*	3	0	3	1
299.0	Markley	*281 Roadcut*	0	0	3	1
298.5	Markley	*Malone Ranch & Antelope*	3	0	1	3
297.1	Archer City	*Andrews*	0	0	1	1
296.5	Archer City	*Sanzenbacher*	1	3	1	1
296.0	Archer City	*Perry 4/5 & Kola Switch*	5	1	0	1
295.8	Archer City	*Kola Switch*	0	1	5	3
295.6	Archer City	*Archer City Bonebed (SS8)*	1	3	0	1
292.4	Nocona	*Coprolite Bonebed*	3	5	1	1
292.0	Nocona	*Copper Mine*	3	5	0	3
288.2	Nocona	*Rattlesnake Canyon*	5	5	0	1
285.9	Nocona	*South of Black Flats*	3	1	0	0
285.0	Nocona	*Parkeys Oil Patch (top Nocona)*	5	3	0	1
284.2	Petrolia	*Parkeys Oil Patch (bottom Petrolia)*	1	3	0	0
284.1	Petrolia	*Godwin Creek, Fire in the Swamp, Fishook Ridge (south), Parkeys Oil Patch*	5	5	0	0
283.9	Petrolia	*Wallace Pocket*	3	5	0	0
283.8	Petrolia	*Spider Hollow*	3	5	0	0
283.7	Petrolia	*Emily Irish*	1	1	5	1
283.3	Petrolia	*Red Hollow*	3	0	1	0
283.2	Petrolia	*Meteor Tank*	5	4	0	0
282.3	Petrolia	*Haycamp Gigantopterid*	3	5	0	0
282.1	Petrolia	*Cowan White's Crossing*	3	3	0	0
281.9	Petrolia	*Castle Hollow redbeds*	5	5	0	0
281.8	Petrolia	*Castle Hollow & Fulda East Road*	1	1	5	0
281.6	Waggoner Ranch	*Fulda Ford Cowan Ranch*	0	1	5	0
281.5	Waggoner Ranch	*Waggoner Ranch New Tank*	4	4	0	0
281.4	Waggoner Ranch	*Boggy Creek*	0	0	0	0
281.0	Waggoner Ranch	*Cowan*	5	4	0	0
280.9	Waggoner Ranch	*Farmer Tank*	3	4	5	0
280.6	Waggoner Ranch	*Tain't A (Franklin Bend vicinity)*	0	5	3	0
280.2	Waggoner Ranch	*Eurypterid, Wattia II, E. of 283N of Wichita River, & Old Lake Kemp Spillway*	3	5	0	0
280.0	Waggoner Ranch	*Mitchell Creek cherts*	1	1	3	0
279.9	Waggoner Ranch	*Mitchell Creek & Crane*	3	0	0	0
279.7	Leuders	*Little Moonshine*	5	5	1	0
279.5	Leuders	*Wattia I*	5	3	1	0
279.1	Clear Fork	*Pony Creek, Grayback, & Harmel Quarry*	3	4	0	0
278.7	Clear Fork	*North Robertson Unit & Brushy Creek*	3	4	0	3

Table S6. continued

Age[1] (Ma)	Formation	Field Locality	Conifers[2]	Peltasperms[2, 3]	Marattialean[2, 4] Ferns	Medullosan[2, 5] Pteridosperms
278.6	Clear Fork	*Hog Creek*	3	4	0	1
277.6	Clear Fork	*North Fork pens*	1	5	0	0
277.5	Clear Fork	*North Robertson Unit & 'Know Where to Park'*	3	5	0	1
277.4	Clear Fork	*Colwell Creek Pond*	3	4	0	0
271.5	San Angelo/Blaine	*Buzzard Peak & East Taylor Pasture*	5	0	0	0
265.0	San Angelo/Blaine	*South Ash Pasture*	5	1	0	0

[1]Ages of fossil plant localities based on stratigraphic age model developed in this study and calibrated to the Geologic Time-Scale 2004 (*S11*).

[2]Abundances given as 'abundant' (present in >50% of specimens examined at site = 5), 'common' (present in >10 to 50% of specimens examined at site = 3), 'rare' (present in up to 10% of specimens examined at site = 1.

[3]Peltasperms include mainly callipterids, comioids, supaioids and gigantopterids.

[4]Marattialean ferns include mainly Pecopteris.

[5]Medullosan pteridosperms include mainly Neuropteris, Alethopteris and Odonopteris. Minor groups (e.g., lycopsids, filicalean ferns, taeniopterids) have been omitted due to low abundance.

REFERENCES

S1. N.J. Tabor, C.J. Yapp, I.P. Montañez, *Geochim. Cosmochim. Acta* **68**, 1503 (2004).

S2. N. J. Tabor, I. P. Montañez, R. J. Southard, *Geochim. Cosmochim. Acta*. **66**, 3093 (2002).

S3. N.J. Tabor, I. P. Montañez, *Palaeogeogr. Palaeoclimatol. Palaeoecol.* **223**, 127 (2005).

S4. N. J. Tabor, *Earth Planetary Science Letters*, (in press).

S5. R. Brewer, *Fabric and Mineral Analysis of Soils* (Krieger, New York, 1976).

S6. P. Deutz, I. P. Montañez, H. C. Monger, *Jour. Sed. Res*. **72**, 809 (2002).

S7. D.J. Beerling *et al.*, *Geochim. Cosmochim. Acta* **66**, 3757 (2002).

S8. G.D. Farquhar, M.H. O'Leary, J.A. Berry, *Aust. J. Plant Physiol*. **9**, 121 (1982).

S9. I.P. Montañez *et al.*, *Palaeogeogr. Palaeoclimatol. Palaeoecol.,* (in review).

S10. C.R. Scotese, PALEOMAP Project, Univ. of Texas, Arlington, TX (1999).

S11. F.M. Gradstein, J.G. Ogg, A.G. Smith, *A Geologic Time-Scale 2004* (Cambridge Univ. Press, 2004).

S12. J. Veizer *et al*., *Chem. Geol.* **161**, 59 (1999).

S13. D.S. Adlis, E.L. Grossman, T.E. Yancey, R.D. McLerran, *Palaios* **3**, 487 (1988).

S14. E.L. Grossman, C.L. Zhang, T.E. Yancey, *Geol. Soc. Am. Bull.* **103**, 953 (1991).

S15. E.L. Grossman, H.S. Mii, T.E. Yancey, *Geol. Soc. Am. Bull.* **105**, 1284 (1993).

S16. H.S. Mii, Ph.D. Thesis, Texas A&M Univ. (1996).

S17. H.S. Mii, E.L, Grossman, T.E. Yancey, *Geology* **25**, 227 (1997).

S18. B.N. Popp, T.F. Anderson, P.A. Sandberg, *Geol. Soc. Am. Bull.* **97**, 1262 (1986).

S19. H.S. Mii, E.L, Grossman, T.E. Yancey, *Geol. Soc. Am. Bull.* **111**, 960 (1999).

S20. H.S. Mii, E.L, Grossman, T.E. Yancey, *Chem. Geol.* **175**, 133 (2001).

S21. P. Bruckschen, S. Oesmann, J. Veizer, *Chem. Geol.* **161**, 127 (1999).

S22. C. Korte, T. Jasper, H.W. Kozur, J. Veizer, *Palaeogeogr. Palaeoclimatol. Palaeoecol.* **224**, 333 (2005).